Growth of Metal Phthalocyanine on Deactivated Semiconducting Surfaces Steered by Selective Orbital Coupling

Sean R. Wagner,[1] Bing Huang,[2] Changwon Park,[2] Jiagui Feng,[1] Mina Yoon,[2,*] and Pengpeng Zhang[1,†]
[1]Department of Physics and Astronomy, Michigan State University, East Lansing, Michigan 48824-2320, USA
[2]Center for Nanophase Materials Sciences, Oak Ridge National Laboratory, Oak Ridge, Tennessee 37831, USA
(Received 19 January 2015; revised manuscript received 8 July 2015; published 26 August 2015)

Using scanning tunneling microscopy and density functional theory, we show that the molecular ordering and orientation of metal phthalocyanine molecules on the deactivated Si surface display a strong dependency on the central transition-metal ion, driven by the degree of orbital hybridization at the heterointerface via selective $p-d$ orbital coupling. This Letter identifies a selective mechanism for modifying the molecule-substrate interaction which impacts the growth behavior of transition-metal-incorporated organic molecules on a technologically relevant substrate for silicon-based devices.

DOI: 10.1103/PhysRevLett.115.096101 PACS numbers: 68.37.Ef, 68.43.Bc, 68.43.Fg, 68.43.Hn

Organic π-conjugated molecules have become emerging materials in the current electronics market for applications including light-emitting diodes [1], field effect transistors [2], and solar cell devices [3]. In these device platforms, molecules are often deposited onto or placed in contact with inorganic surfaces. Thus, the resultant device performances are highly correlated with the electronic structure, molecular orientation, and molecular ordering at the heterointerface [2–8]. This has stimulated intense interest in understanding and further tuning the interfacial electronic structure and the molecule-substrate interaction that governs the organic molecular growth [8–19].

Metal phthalocyanine (*M*Pc) is one of the most frequently studied planar molecules in organic molecular thin film growth on a variety of insulating, semiconducting, and more commonly, metallic surfaces [8,12–38]. Of them, metallic substrates provide more flexibility in tuning the *M*Pc-substrate interaction through orbital hybridization and charge redistribution associated with the central transition-metal (TM) ion [16,20,21]. Nevertheless, this tunable hybridization has little influence on the orientation and ordering of *M*Pc molecules at the heterointerface, where close-packed flat-lying molecular structures are often observed in the first monolayer which, then, gradually relax into bulk configured molecular packing in multilayers [17,22,23,25]. Semiconducting substrates, on the other hand, provide a particular challenge to self-assemble organic molecules on top due to the existence of surface dangling bonds which localize molecules and prevent them from forming ordered structures. To circumvent this problem, the surface needs to be atomically passivated, such as through hydrogen termination. However, if the intermolecular interaction dominates the growth, a bulk configured polycrystalline or polymorphic film will form, which is not ideal for electronic applications [34].

Recently, it has been shown that the deactivated Si(111)-B $\sqrt{3}\times\sqrt{3}$ $R30°$ surface possesses a clean band gap and facilitates the long-range ordered growth of ZnPc (TM = Zn) in both the in-plane and out-of-plane directions [12,14]. However, to date, there is still a lack of understanding of the underlying molecule-substrate binding mechanism and the origin of this long-range ordered growth at the molecular level. Also, to what extent the molecule-substrate coupling strength can be rationally tuned and how it impacts the potential landscape, which is critical for controlling the growth kinetics and the thin film morphology, remain to be explored.

In this Letter, via scanning tunneling microscopy (STM) experiments and density functional theory (DFT) calculations, we show that the molecular ordering and orientation of the prototypical *M*Pc molecules on the deactivated Si(111)-B surface can be drastically altered by the coordinated TM ion within the *M*Pc molecule. The localized p_z orbitals on top Si adatoms (ad-Si) facilitate highly selective orbital coupling with the d orbitals of the TM ion, leading to varied molecule-substrate coupling strengths. Additionally, the significantly large lattice parameter of Si(111)-B, two or three times larger than those of metallic and insulating surfaces typically utilized in *M*Pc studies, provides a more corrugated potential energy landscape that is further tailored by the TM ion–ad-Si coupling to impact the molecular packing and orientation. These discoveries pave the way for understanding the assembly and growth phenomena of TM-incorporated organic molecules on a technologically relevant substrate for silicon-based devices.

We utilize heavily boron doped Si(111) substrates where subsurface boron segregation ($\sim 1/3$ monolayer) is induced by an extended sample annealing at 800 °C [39]. Each subsurface trivalent boron atom bonds to four neighboring Si atoms, thus, allowing for the depletion of unpaired electrons from the ad-Si. This process yields an atomically smooth and deactivated Si(111)-B $\sqrt{3}\times\sqrt{3}$ $R30°$ surface with a clean band gap (Fig. S1 [39]), suitable for self-assembly of organic molecules [52,53].

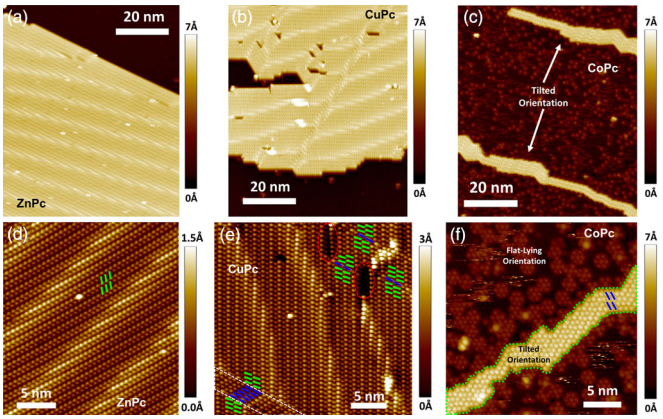

FIG. 1 (color online). (a)–(c) Large scale STM topography images of submonolayer coverage of (a) ZnPc, (b) CuPc, and (c) CoPc deposited on the deactivated Si surface at the same condition. (d)–(f) Expanded STM topography images of (d) ZnPc, (e) CuPc, and (f) CoPc showing the packing of *M*Pc molecules within a typical domain. ZnPc exhibits the highly ordered tilted molecular configuration. CuPc displays shifts in the molecular packing which are outlined by the dashed white lines and gap defects as highlighted by the dashed red ovals. CoPc shows both tilted and flat-lying molecular orientations, with the tilted domain outlined by the dashed green lines. The green and blue bars in (d)–(f) represent individual Pc molecules with tilted orientation. Molecular assignment in (f) is further corroborated in Fig. S2 [39]. Scanning conditions for (a)–(f): $V_s = +2.0$–2.5 V, $I_t = 4$–30 pA.

Figures 1(a)–1(f) present the surface topography of various *M*Pc molecules deposited on the deactivated Si(111)-B surface with $M =$ Zn, Cu, and Co, respectively, where distinct molecular assembly and growth behaviors are clearly identified. As shown in Figs. 1(a) and 1(d), ZnPc molecules adopt a tilted molecular configuration and crystallize to form densely packed structures (extensive discussion regarding this molecular packing can be found in Refs. [12] and [14]). To guide the view, green bar markers are included in the zoomed in STM image [Fig. 1(d)] of a highly ordered ZnPc domain to represent individual ZnPc molecules with tilted orientation. For CuPc, although it preserves the identical molecular orientation and packing motif as ZnPc [12–14], a notable degradation of the film quality is observed where a significant amount of gap defects and shifts in the molecular packing occur within the molecular domains [Figs. 1(b) and 1(e)] [39]. The zoomed in STM image [Fig. 1(e)] clearly illustrates that these shifts, as highlighted by the green and blue bars as well as the region outlined by dashed white lines, result in the zigzag patterned growth which can also lead to the development of gap defects nearby as outlined by the dashed red ovals. Intriguingly, for the CoPc growth, we find that the molecules predominantly lie flat on the surface while the molecular patches with tilted configuration only emerge and are sparsely dispersed among the flat-lying molecules when the coverage is increased above a certain threshold, as illustrated in Figs. 1(c) and 1(f). The high degree of disorder in the CoPc molecular growth on a small scale continues to be prevalent when mapping the topography on larger scales. Such a drastically different molecular assembly and growth behavior observed for various *M*Pc deposited on the Si(111)-B surface is in sharp contrast to the growth of these molecules on metallic surfaces where close-packed flat-lying molecular structures are formed regardless of the choice of the central TM ion [17,22,23]. These results suggest that the critical interactions governing the molecular growth, i.e., the molecule-substrate and molecule-molecule interactions, might be mediated by the central TM ion in *M*Pc.

This is further corroborated by the difference observed in the initial molecular adsorption on the Si(111)-B surface. For ZnPc molecules, once deposited they are able to diffuse rapidly across the Si terraces and nucleate at the energetically favorable Si step edge sites [12–15]. Thus, single flat-lying ZnPc molecules could not be readily observed unless localized on a defect site on the Si terrace. Substituting Cu for Zn, we find that, although molecules still exhibit a large diffusivity, there is a notable increase in the nucleation of flat-lying molecules between tilted molecular domains which exceeds the expected defect density [a typical STM image is shown in Fig. 2(a)]. In Fig. 2(c), one can clearly identify the four benzene rings of an individual CuPc molecule with the central Cu metal ion appearing as a depression [22]. Detailed analysis of a collection of STM images indicates that CuPc molecules display nonspecific site registration with the deactivated Si surface. In contrast, for the case of CoPc, both the Co ions, which appear as bright protrusions in STM images due to orbital-mediated tunneling [22,54], and the four benzene rings, preferentially register with the ad-Si atoms, as illustrated in Figs. 2(b) and 2(d). The symmetry of the CoPc molecule is reduced from C_4 to C_2 in order to maximize the adsorption energy (see Sec. IV in the Supplemental Material [39]). Because of the high degree of molecular registration with the underlying surface (C_6 symmetry) along the common symmetry elements, as highlighted by the dashed and solid red, blue, and green rectangles in Fig. 2(b), only three stable flat-lying CoPc orientations are observed. The dashed white circle depicts a single molecule rotating (fast tunneling) between all three configurations triggered by the STM tip [55]. The combined individual molecule and large scale molecular growth suggest a strong molecule-substrate interaction between CoPc and the deactivated Si(111)-B surface.

It is known that the crystal field induced by the D_{4h} symmetry of the free-standing *M*Pc molecules gives rise to the *d*-orbital splitting of its central TM ion into a doubly degenerate state (d_{xz}, d_{yz}) and three singly degenerate states (d_{xy}, $d_{x^2-y^2}$, and d_{z^2}) where d_{xz}, d_{yz}, and d_{z^2} protrude from the molecular plane [56,57]. As illustrated in Fig. 3(a), by changing the TM ion from Zn to Co, the charge distribution

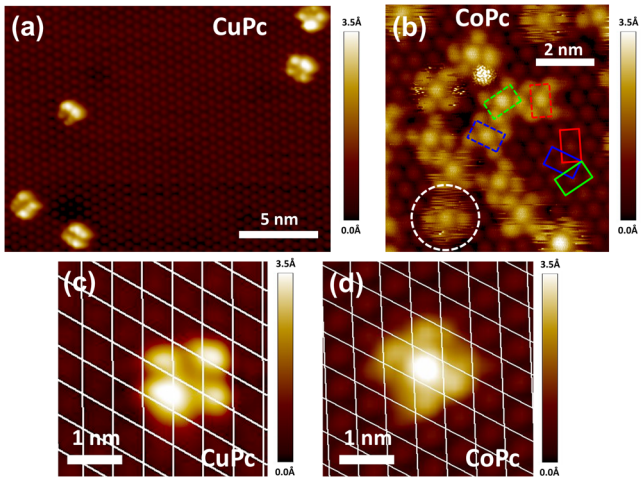

FIG. 2 (color online). (a) and (b), STM topography images of flat-lying (a) CuPc and (b) CoPc molecules taken in regions between tilted molecular domains. The three stable flat-lying CoPc orientations allowed by the substrate symmetry are highlighted by the red, blue, and green dashed rectangles, exhibiting registration with the underlying surface (solid rectangles). The dashed white circle highlights a single molecule rotating between all three orientations. (c) and (d), STM topography image of a single flat-lying CuPc molecule (c), and CoPc molecule (d) on the deactivated Si surface (overlaid unit cell grid). Scanning conditions for (a)–(d): $V_s = +1.3$–2.0 V [$V_s = -2.0$ V in (c)], $I_t = 3$–25 pA.

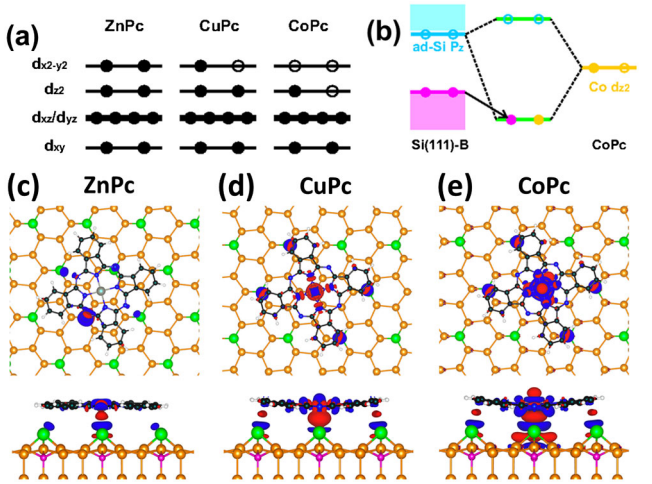

FIG. 3 (color online). (a) Schematic diagram of d-orbital filling for ZnPc, CuPc, and CoPc. (b) Schematic diagram of the orbital hybridization mechanism between a CoPc molecule and the Si(111)-B surface. Note that the back-bond surface state (the discrete energy level in pink) is in resonance with the bulk Si valence band. (c)–(e) Calculated charge density difference maps shown for the molecular adsorption of (c) ZnPc, (d) CuPc, and (e) CoPc on the deactivated Si surface. The same isosurface charge density value (± 0.001 e/Bohr^3) is selected for all of these plots. Red regions denote electron accumulation while blue regions indicate electron depletion. The green balls represent ad-Si, and pink balls for subsurface borons.

within each orbital is altered and a depopulated d_{z^2} orbital is formed in CoPc [57,58]. In order to understand the mechanism of molecular binding to the substrate mediated by the d-orbital filling and to account for the contrasting molecular adsorption and growth behavior of MPc on the deactivated Si(111)-B surface, we perform DFT calculations within the generalized gradient approximation as implemented in the Vienna *ab initio* simulation package (VASP) [59]. The Perdew-Burke-Ernzerhof (PBE) functional is selected in our calculations with the projector augmented wave potentials applied to describe the core electrons. The effect of van der Waals (vdW) interactions is taken into account by using the PBE + vdW scheme where self-consistent electron density is utilized to calculate C6 coefficients [60]. In our calculations, structural parameters are allowed to fully relax until the force on each atom is less than 0.02 eV/Å. For more details regarding the calculation techniques utilized in this Letter, refer to Sec. I in the Supplemental Material [39].

Figure 3(b) presents the key mechanism of selective orbital hybridization between the singly occupied d_{z^2} orbital of CoPc and the empty p_z orbital of ad-Si. The d_{z^2} orbital, which is strongly localized on the central TM ion (over 90% of the molecular orbital) based on our DFT calculations, is the only symmetry-allowed orbital having nonzero overlap with the p_z state of ad-Si (see Fig. S3 and Sec. III in the Supplemental Material [39]). Thus, a strong bond is anticipated to form between the singly occupied d_{z^2} orbital of CoPc and the ad-Si, leading to a significantly higher energy gain as compared to the case of ZnPc and CuPc. As illustrated in Fig. 3(b), the energy level of the ad-Si p_z orbital is located near the bulk Si conduction band minimum [61], while the Co d_{z^2} orbital is located inside the bulk Si band gap. Once CoPc is adsorbed on the surface, the selective $p - d$ orbital coupling mechanism results in a hybridized $p_z - d_{z^2}$ bonding state, which is lower in energy than the bulk Si valence band maximum. As a result, one electron is transferred from the substrate to the bonding state, making it fully occupied. This hybridization effect is also manifested in the charge density difference plot upon the adsorption of MPc on the substrate. The magnitude of the charge redistribution is determined by the degree of mixing between the p_z orbital of ad-Si and the d_{z^2} orbital of MPc, which is set by the energy level difference between the two (see Sec. III in the Supplemental Material [39]). As presented in Figs. 3(c)–3(e), the strong orbital hybridization introduces a significant charge accumulation on the p_z orbitals of ad-Si for CoPc [red regions in Fig. 3(e)], while a negligible or minute charge accumulation is observed for ZnPc and CuPc, respectively [Figs. 3(c) and 3(d)]. It is important to note that, in order to distinguish the interaction schemes between the central TM ion and the ad-Si in these molecular systems, the ZnPc and CuPc molecular configuration in Figs. 3(c) and 3(d) (in one of its local energetic minima) are selected purposely to be comparable to that of

CoPc [Fig. 3(e)] in the calculations (see Fig. S5(b) and Sec. IV in the Supplemental Material [39]). Also, note that the net charge transfer from the substrate to CoPc and ZnPc is zero based on our occupancy analysis, while in the case of CuPc, the charge donation to the empty p_z state is balanced with the partial charge backdonation from the substrate to the $d_{x^2-y^2}$ orbital, resulting in a small amount of net charge ($<0.1e$).

Thus far, we have identified a distinct mechanism of molecular binding to the substrate mediated by the central TM ions. To further investigate the interplay between molecule-substrate interaction and molecular growth, the potential energy landscape of the surface is examined along selective directions where the internal molecular coordination (including rotation) is fully optimized at each point. For CuPc (similar trends are expected for ZnPc), two linearly independent diffusion pathways are identified [inset in Fig. 4(a)] for a given initial molecular orientation and the potential along each line is presented in Fig. 4(a). Along both pathways, there are many local minima separated by low potential barriers that are mainly due to the vdW energy corrugation which arises from the adaptive relaxation of the CuPc molecule, as well as from the weak interaction between the ad-Si and the nitrogen atoms of the Pc molecule (see Sec. IV in the Supplemental Material [39]). Nevertheless, these small diffusion energy barriers can be easily overcome by intermolecular attraction, resulting in unhindered molecular diffusion of CuPc on the deactivated Si(111) surface. In contrast, in the case of CoPc, the potential energy landscape along the easiest path (solid) exhibits a deep potential well associated with a significant energy barrier that is over 1.2 eV [Fig. 4(b)]. The small vdW potential energy corrugation (solid red line) indicates that this large energy barrier originates from the breaking of the chemical bond between the Co and the ad-Si atom as discussed previously. This chemical bond dominates the potential energy landscape and results in a strong localization of molecules on the surface as observed in Figs. 2(b) and 2(d).

Last, we would like to reiterate the unique aspects of the Si(111)-B surface which leads to the intriguing molecular growth phenomena that have not been previously observed on metallic substrates. The major difference between the metallic and Si(111)-B surface is the potential energy landscape, specifically its corrugation and homogeneity. The degree of the potential corrugation of *M*Pc on a metallic surface, as corroborated for the case of Au (111), is typically an order of magnitude smaller than that of even weakly interacting ZnPc or CuPc on the Si(111)-B surface (Fig. S6 [39]). As a result, with increasing molecular coverage, the energy gain from the intermolecular interaction can be fully achieved on a metallic surface due to its flat potential energy landscape, driving the formation of close-packed flat-lying *M*Pc molecular structures on the surface [17,19,22]. However, the significant

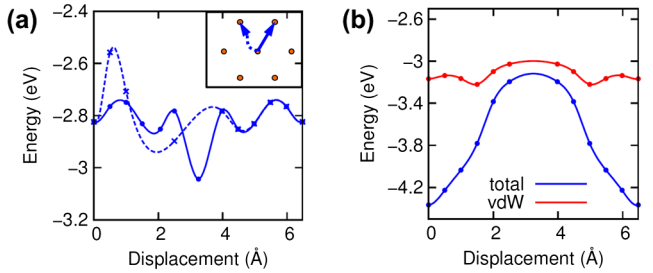

FIG. 4 (color online). (a) The energy landscapes of CuPc along the different diffusion pathways. Lines connecting the data points are shown to guide the view. Inset: Depicts the linearly independent minimum energy pathways for molecular diffusion. Orange circles denote the positions of ad-Si. Depending on the initial molecular orientation, the roles of the two pathways can be exchanged. (b) The energy landscape of CoPc along the solid path as shown in inset in (a).

potential corrugation of Si(111)-B requires that the *M*Pc molecules must first adsorb at the sites of local energy minima. As the molecular coverage on the Si(111)-B surface increases, these low energy sites will become occupied, leaving unfavorable adsorption sites for incoming *M*Pc molecules. Therefore, if the molecule-substrate interaction is weak in comparison to the molecule-molecule interaction, as for the case of ZnPc and CuPc (Table I), it is energetically more beneficial to maximize the $\pi-\pi$ intermolecular attraction at a cost of a portion of the surface adsorption energy, leading to a structural transition to a tilted molecular configuration [12–15]. However, for CoPc, the molecule-Si binding energy is significantly larger than the intermolecular binding energy (Table I), enabling the majority of the molecules to adopt the flat-lying orientation [Figs. 1(c) and 1(f)]. Furthermore, the large diffusion barrier experienced by the CoPc molecules also prevents them from forming long-range ordered domains.

In summary, we have shown that the localized p_z orbitals on the Si(111)-B surface allow for highly selective orbital coupling with the d orbitals of *M*Pc molecules. By appropriately choosing the coordinated TM ion in *M*Pc to modulate the strength of the $p-d$ orbital hybridization and the overall potential corrugation, molecular orientation and ordering at the heterointerface can be drastically altered. The significance of the $p-d$ orbital hybridization may also be manifested in other TM based molecular systems, such as porphyrins, and other technologically significant surfaces including topological insulators [38].

Experiment work was supported by the U.S. Department of Energy Office of Science Early Career Research Program (Grant No. DE-SC0006400) through the Office of Basic Energy Sciences. Theory work (C. P. and M. Y.) was conducted at the Center for Nanophase Materials Sciences, which is sponsored at Oak Ridge National Laboratory by the Scientific User Facilities Division, Office of Basic Energy Sciences, U.S. Department of

TABLE I. *M*Pc-Si and *M*Pc-*M*Pc binding energy (BE).

*M*Pc type	*M*Pc-Si BE (eV)	α phase [62] BE (eV)	β phase [62] BE (eV)
ZnPc	3.18	3.92	4.00
CuPc	3.04	3.85	3.88
CoPc	4.37	3.90	4.00

Energy and partly (B. H.) supported by the Materials Sciences and Engineering Divisions, Office of Basic Energy Sciences, U.S. Department of Energy. This research used resources of the National Energy Research Scientific Computing Center, supported by the Office of Science of the U.S. Department of Energy under Contract No. DE-AC02-05CH11231. The authors thank R. R. Lunt and C. J. Traverse for aiding in the molecular purification process.

S. R. W., B. H., and C. P. contributed equally to this work.

*myoon@ornl.gov
†zhang@pa.msu.edu

[1] L. S. Hung and C. H. Chen, Mater. Sci. Eng. R **39**, 143 (2002).
[2] Y.-Y. Noh, J.-J. Kim, Y. Yoshida, and K. Yase, Adv. Mater. **15**, 699 (2003).
[3] Z.-X. Xu, V. A. L. Roy, Z.-T. Liu, and C. S. Lee, Appl. Phys. Lett. **97**, 163301 (2010).
[4] A. B. Chwang and C. D. Frisbie, J. Appl. Phys. **90**, 1342 (2001).
[5] J. Hwang, A. Wan, and A. Kahn, Mater. Sci. Eng. R **64**, 1 (2009).
[6] R. R. Lunt, J. B. Benziger, and S. R. Forrest, Adv. Mater. **22**, 1233 (2010).
[7] S. Duhm, G. Heimel, I. Salzmann, H. Glowatzki, R. L. Johnson, A. Vollmer, J. P. Rabe, and N. Koch, Nat. Mater. **7**, 326 (2008).
[8] K. Xiao *et al.*, J. Am. Chem. Soc. **135**, 3680 (2013).
[9] L. Bartels, Nat. Chem. **2**, 87 (2010).
[10] T.-C. Tseng *et al.*, Nat. Chem. **2**, 374 (2010).
[11] G. Heimel *et al.*, Nat. Chem. **5**, 187 (2013).
[12] S. R. Wagner, R. R. Lunt, and P. P. Zhang, Phys. Rev. Lett. **110**, 086107 (2013).
[13] S. R. Wagner and P. P. Zhang, Mater. Res. Soc. Symp. Proc. **1550**, 609 (2013).
[14] S. R. Wagner and P. P. Zhang, J. Phys. Chem. C **118**, 2194 (2014).
[15] S. R. Wagner and P. P. Zhang, Surf. Sci. **630**, 22 (2014).
[16] A. Mugarza, R. Robles, C. Krull, R. Korytár, N. Lorente, and P. Gambardella, Phys. Rev. B **85**, 155437 (2012).
[17] S. C. Bobaru, E. Salomon, J.-M. Layet, and T. Angot, J. Phys. Chem. C **115**, 5875 (2011).
[18] W. Dou, S. Huang, R. Q. Zhang, and C. S. Lee, J. Chem. Phys. **134**, 094705 (2011).
[19] C. Stadler, S. Hansen, I. Kröger, C. Kumpf, and E. Umbach, Nat. Phys. **5**, 153 (2009).
[20] Y. Y. Zhang, S. X. Du, and H.-J. Gao, Phys. Rev. B **84**, 125446 (2011).
[21] Y. L. Huang, E. Wruss, D. A. Egger, S. Kera, N. Ueno, W. A. Saidi, T. Bucko, A. T. S. Wee, and E. Zojer, Molecules **19**, 2969 (2014).
[22] X. Lu, K. W. Hipps, X. D. Wang, and U. Mazur, J. Am. Chem. Soc. **118**, 7197 (1996).
[23] Q. Guo, Z. Qin, K. Zang, C. Liu, Y. Yu, and G. Cao, Langmuir **26**, 11804 (2010).
[24] J. Uihlein, H. Peisert, M. Glaser, M. Polek, H. Adler, F. Petraki, R. Ovsyannikov, M. Bauer, and T. Chassé, J. Chem. Phys. **138**, 081101 (2013).
[25] S. Söhnchen, S. Lukas, and G. Witte, J. Chem. Phys. **121**, 525 (2004).
[26] K. Yang, W. D. Xiao, Y. H. Jiang, H. G. Zhang, L. W. Liu, J. H. Mao, H. T. Zhou, S. X. Du, and H.-J. Gao, J. Phys. Chem. C **116**, 14052 (2012).
[27] S. K. Hämäläinen, M. Stepanova, R. Drost, P. Liljeroth, J. Lahtinen, and J. Sainio, J. Phys. Chem. C **116**, 20433 (2012).
[28] P. Järvinen, S. K. Hämäläinen, M. Ijäs, A. Harju, and P. Liljeroth, J. Phys. Chem. C **118**, 13320 (2014).
[29] M. Scardamaglia, C. Struzzi, S. Lizzit, M. Dalmiglio, P. Lacovig, A. Baraldi, C. Mariani, and M. G. Betti, Langmuir **29**, 10440 (2013).
[30] Y.-L. Wang *et al.*, Phys. Rev. B **82**, 245420 (2010).
[31] L. Ramoino, M. von Arx, S. Schintke, A. Baratoff, H.-J. Güntherodt, and T. A. Jung, Chem. Phys. Lett. **417**, 22 (2006).
[32] A. Scarfato, S.-H. Chang, S. Kuck, J. Brede, G. Hoffmann, and R. Wiesendanger, Surf. Sci. **602**, 677 (2008).
[33] Y. Wang, J. Kröger, R. Berndt, and H. Tang, J. Am. Chem. Soc. **132**, 12546 (2010).
[34] M. Nakamura, T. Matsunobe, and H. Tokumoto, J. Appl. Phys. **89**, 7860 (2001).
[35] A. C. Brieva, T. E. Jenkins, D. G. Jones, F. Strössner, D. A. Evans, and G. F. Clark, J. Appl. Phys. **99**, 073504 (2006).
[36] A. C. Mayer, R. Ruiz, H. Zhou, R. L. Headrick, A. Kazimirov, and G. G. Malliaras, Phys. Rev. B **73**, 205307 (2006).
[37] A. R. Woll, T. V. Desai, and J. R. Engstrom, Phys. Rev. B **84**, 075479 (2011).
[38] T. Bathon, P. Sessi, K. A. Kokh, O. E. Tereshchenko, and M. Bode, Nano Lett. **15**, 2442 (2015).
[39] See Supplemental Material at http://link.aps.org/supplemental/10.1103/PhysRevLett.115.096101 for methods summary, supplementary figures, and additional discussion, which includes Refs. [40–51].
[40] N. Marom, O. Hod, G. E. Scuseria, and L. Kronik, J. Chem. Phys. **128**, 164107 (2008).
[41] J. D. Baran, J. A. Larsson, R. A. J. Woolley, Y. Cong, P. J. Moriarty, A. A. Cafolla, K. Schulte, and V. R. Dhanak, Phys. Rev. B **81**, 075413 (2010).
[42] J. D. Baran and J. A. Larsson, J. Phys. Chem. C **117**, 23887 (2013).
[43] T. G. Gopakumar, T. Brumme, J. Kröger, C. Toher, G. Cuniberti, and R. Berndt, J. Phys. Chem. C **115**, 12173 (2011).
[44] G. Di Santo, C. Castellarin-Cudia, M. Fanetti, B. Taleatu, P. Borghetti, L. Sangaletti, L. Floreano, E. Magnano, F. Bondino, and A. Goldoni, J. Phys. Chem. C **115**, 4155 (2011).

[45] T. Lukasczyk, K. Flechtner, L. R. Merte, N. Jux, F. Maier, J. M. Gottfried, and H.-P. Steinrück, J. Phys. Chem. C **111**, 3090 (2007).
[46] F. Buchner, K.-G. Warnick, T. Wölfle, A. Görling, H.-P. Steinrück, W. Hieringer, and H. Marbach, J. Phys. Chem. C **113**, 16450 (2009).
[47] W. Auwärter *et al.*, Phys. Rev. B **81**, 245403 (2010).
[48] P. Sessi, T. Bathon, K. A. Kokh, O. E. Tereshchenko, and M. Bode, Nano Lett. **14**, 5092 (2014).
[49] N. Marom and L. Kronik, Appl. Phys. A **95**, 159 (2009).
[50] R. Cuadrado, J. I. Cerdá, Y. Wang, G. Xin, R. Berndt, and H. Tang, J. Chem. Phys. **133**, 154701 (2010).
[51] S.-H. Chang, S. Kuck, J. Brede, L. Lichtenstein, G. Hoffmann, and R. Wiesendanger, Phys. Rev. B **78**, 233409 (2008).
[52] I.-W. Lyo, E. Kaxiras, and Ph. Avouris, Phys. Rev. Lett. **63**, 1261 (1989).
[53] A. V. Zotov, M. A. Kulakov, S. V. Ryzhkov, A. A. Saranin, V. G. Lifshits, B. Bullemer, and I. Eisele, Surf. Sci. **345**, 313 (1996).
[54] L. Scudiero, D. E. Barlow, U. Mazur, and K. W. Hipps, J. Am. Chem. Soc. **123**, 4073 (2001).
[55] B. C. Stipe, M. A. Rezaei, and W. Ho, Science **279**, 1907 (1998).
[56] Y. Nishida and S. Kida, Coord. Chem. Rev. **27**, 275 (1979).
[57] M.-S. Liao and S. Scheiner, J. Chem. Phys. **114**, 9780 (2001).
[58] W. A. Harrison, *Electronic Structure and the Properties of Solids* (Dover Publications, New York, 1989).
[59] G. Kresse and J. Furthmüller, Comput. Mater. Sci. **6**, 15 (1996).
[60] A. Tkatchenko and M. Scheffler, Phys. Rev. Lett. **102**, 073005 (2009).
[61] E. Kaxiras, K. C. Pandey, F. J. Himpsel, and R. M. Tromp, Phys. Rev. B **41**, 1262 (1990).
[62] The α and β phases are two commonly observed bulk *M*Pc packing configurations [see Acta Crystallogr. Sect. A **37**, 692 (1981)] which were used to calculate the intermolecular binding energy shown in Table I.